Liquid Crystals
Publication details, including instructions for authors and subscription information:
http://www.informaworld.com/smpp/title~content=t713926090

Cubic phases of 4'-*n*-alkoxy-3'-nitrobiphenyl-4-carboxylic acids (ANBC-*n*)

Shoichi Kutsumizu; Koushi Morita; Tatsuya Ichikawa; Shinichi Yano; Shuichi Nojima; Takanari Yamaguchi

Online publication date: 11 November 2010

To cite this Article Kutsumizu, Shoichi , Morita, Koushi , Ichikawa, Tatsuya , Yano, Shinichi , Nojima, Shuichi and Yamaguchi, Takanari(2002) 'Cubic phases of 4'-*n*-alkoxy-3'-nitrobiphenyl-4-carboxylic acids (ANBC-*n*)', Liquid Crystals, 29: 11, 1447 — 1458
To link to this Article: DOI: 10.1080/02678290260372646
URL: http://dx.doi.org/10.1080/02678290260372646

LIQUID CRYSTALS, 2002, VOL. 29, NO. 11, 1447–1458

Cubic phases of 4′-*n*-alkoxy-3′-nitrobiphenyl-4-carboxylic acids (ANBC-*n*)

SHOICHI KUTSUMIZU*, KOUSHI MORITA, TATSUYA ICHIKAWA, SHINICHI YANO

Department of Chemistry, Faculty of Engineering, Gifu University, 1-1 Yanagido, Gifu 501-1193, Japan

SHUICHI NOJIMA

School of Materials Science, Japan Advanced Institute of Science and Technology (JAIST), 1-1 Asahidai, Tatsunokuchi, Nomi, Ishikawa 923-1292, Japan; Graduate School of Science and Engineering, Tokyo Institute of Technology, 2-12-2 O-okayama, Meguro-ku, Tokyo, 152-8552, Japan

and TAKANARI YAMAGUCHI

Tsukuba Research Laboratory, Sumitomo Chemical Co., Ltd., 6 Kitahara, Tsukuba, Ibaraki 300-3266, Japan

(*Received 2 April 2002; in final form 3 July 2002; accepted 19 July 2002*)

The structure of the thermotropic cubic phases of 4′-*n*-alkoxy-3′-nitrobiphenyl-4-carboxylic acids (ANBC-*n*, where *n* indicates the number of carbon atoms in the alkoxy group) was studied by X-ray diffraction. For the homologues with $n = 15$, 16, 17, and 18, the cubic phase was of an $Ia3d$ type, whereas the homologues with $n = 19$, 20, and 21 exhibited an $Im3m$ cubic structure; for these seven homologues the same type of cubic structure was observed both on heating and cooling. Further lengthening of the alkoxy chain to $n = 22$ and 26, however, gave two types of cubic structure in the cubic phase region on heating, one with $Im3m$ symmetry in the low temperature region and the other with $Ia3d$ symmetry in the high temperature region. On cooling, the two homologues exhibited the $Ia3d$ cubic structure only. This is the first example in the cubic phase region of a series of homologues containing two types of structure, dependent on temperature and *n*. Such a complicated phase diagram in the cubic region is clearly understood qualitatively in terms of Gibbs free energy–temperature diagrams. The dependence of structural parameters such as the cubic lattice constant on the alkoxy chain length *n* are also presented and discussed.

1. Introduction

Thermotropic cubic liquid crystalline phases are one of the most fascinating phases in the field of liquid crystals, in that some kinds of optically anisotropic rod-like molecule form an optically isotropic organization in a certain temperature range, neighboured by other anisotropic phases with lamellar, hexagonal, or columnar structures [1]. The same type of phase is seen in lyotropic systems such as lipid–solvent systems [2] and also in the field of block copolymers [3]. Regardless of the diversity of chemical systems exhibiting cubic phases, they share the common feature of consisting of two incompatible components, e.g. aliphatic vs aromatic, apolar vs polar, or soft vs hard components, with a ratio of one component to the other greater than 1. Our understanding in this field is, however, still far from complete and systematic studies are needed to elucidate the key factors governing the transitions between those cubic and other anisotropic phases and the relationship between the structural unit and the cubic structure formed.

4′-*n*-Alkoxy-3′-nitrobiphenyl-4-carboxylic acids (designated as ANBC-*n*, see the structure) are well known for exhibiting one of the thermotropic cubic phases, labelled cubic D (CubD) [4–31]. The phase behaviour of ANBC-*n* and the structure of the CubD phase have been investigated by optical microscopy [4, 5, 9, 17], refractivity [6], X-ray diffraction [7, 8, 12, 14, 16, 21, 25, 27, 28, 31], NMR [13, 20], viscoelastic measurements [18, 23], infrared spectroscopy [19, 26], adiabatic calorimetry

*Author for correspondence; e-mail: kutsu@cc.gifu-u.ac.jp

Liquid Crystals ISSN 0267-8292 print/ISSN 1366-5855 online © 2002 Taylor & Francis Ltd
http://www.tandf.co.uk/journals
DOI: 10.1080/0267829021000026069

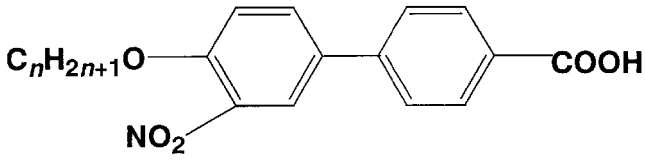

Structure. Chemical structure of ANBC-n.

[22, 24, 29, 30] and so on. The number of carbon atoms in the alkoxy group, n, is a key factor for forming the CubD phase; the CubD phase appears when $n \geqq 15$, and the temperature region widens monotonously with increasing n [17]. For $n = 16$ and 18, the space group of the phase has already been identified as $Ia3d$ [8, 16, 21] and it was reasonably assumed at that time that the space group of the remaining homologues would be the same.

Recently, we found that one homologue having a very long alkoxy chain, $n = 26$, forms two types of cubic phase, one with $Im3m$ and the other with $Ia3d$ symmetry, and the $Im3m$ cubic phase is transformed into the $Ia3d$ cubic phase at 435 K on heating [25, 28]. This was the first example of a thermotropic cubic–cubic phase transition in a one-component system, although a few examples have been reported in lyotropic binary or ternary mixtures, where the phase behaviour is a function of the water content [2, 32, 33]. Moreover, this finding, which was accomplished by using a high resolution, small angle X-ray scattering (SAXS) apparatus, obliged us to re-examine the space group of the cubic phases of other homologues than $n = 16$, 18 and 26.

This paper reports the phase type as a function of temperature (T) and alkoxy chain length n in the region labelled CubD. An attempt is made to interpret the behaviour in terms of Gibbs free energy (G)–T diagrams. The dependence of structural parameters such as the cubic lattice constant on the alkoxy chain length n is also presented and discussed. Part of the results was presented at ILCC 2000 in Sendai [31].

2. Experimental

2.1. *Preparation*

The ANBC-n compounds were prepared according to the method of Gray *et al.* [4, 34]. The samples were recrystallized from ethanol several times and confirmed as fully pure by infrared (IR), ^{1}H NMR, mass spectroscopy (MS), thin layer chromatography, differential scanning calorimetry (DSC), and elemental analysis.

2.2. *Measurements*

IR spectra were recorded with a Perkin-Elmer 1640 and a Perkin-Elmer system 2000 Fourier transform IR spectrometer. ^{1}H NMR and MS spectra were recorded using a JEOL JNM-α400 spectrometer and a Shimadzu GCMS QP-1000 system, respectively. The phase transitions and thermal stability were examined using a Seiko Denshi DSC-210 and TG/DTA-300 interfaced to a TA data station (SSC 5000 system). The measurements were performed under a dry N_2 flow of *c.* 40 ml min^{-1} for DSC and of *c.* 200 ml min^{-1} for TG/DTA; the scanning rate was 5 K min^{-1} for both measurements. The texture of each mesophase was observed using a Nikon Optiphot-pol XTP-11 polarizing optical microscope (POM) equipped with a Mettler FP82 hot stage and a Mettler FP80 central processor at a heating/cooling rate of 5 K min^{-1}.

X-ray diffraction (XRD) patterns at elevated temperatures were obtained from powder samples contained in thin glass capillaries of 1.5 mm diameter which were placed in a Mettler FP82HT hot stage, and the temperature was controlled within ± 0.1 °C by a Mettler FP90 central processor. The accuracy of the temperature was checked by using a calibrated Fe–constantan thermocouple. The following two set-ups were used.

(a) A MAC Science X-ray generator (M18XHF) was operated with a copper target at 40 kV and 30 mA, and the CuKα radiation ($\lambda = 0.154$ nm) was point-focused with Huxley–Holms optics. The scattered X-rays were detected by a one-dimensional proportional counter (PSPC) with an effective length of 10 cm. The distance between the sample and the PSPC was about 40 cm, and the geometry was further checked using chicken tendon collagen, which gives a set of sharp diffractions corresponding to a spacing of 65.3 nm, and by α-stearic acid giving a set of diffractions for 3.95 nm. The accumulation time for each measurement was 500–3600 s, depending on the intensity obtained and the quality needed.

(b) A Rigaku R-AXIS IIC X-ray system was used and operated with a copper target at 40 kV and 150 mA, and the CuKα radiation was collimated into the sample capillary. The scattered X-rays were recorded on a two-dimensional imaging plate (IP) camera with an effective area of 20×20 cm^2; the camera distance was 20 cm. The exposure time for each measurement was 5–10 min.

Viscoelastic measurements were performed by using a Rheometric Dynamic Stress Rheometer RDS-II. The parallel plate shear geometry was employed and the samples were sandwiched between two plates at a temperature above the melting point under a N_2 gas atmosphere. The diameter of the plate and the gap between the two plates were 25 and 1 mm, respectively. In the isochronal experiments, the rate of heating was 1 K min^{-1}, and the strain amplitude was maintained at less than 0.5%.

3. Results

Figure 1 shows the phase diagram for each ANBC-n. The cubic phase is formed for the homologues with $n \geqq 15$. As the alkoxy chain length n is increased, the smectic C (SmC) to Cub phase transition temperature falls monotonously, while the Cub to smectic A (SmA) (or a structured liquid I_1) [9, 11, 17, 28] phase transition temperature is almost independent of n; as a result, the temperature region of the Cub phase widens with increasing n. Thus, it can be said that the Cub phase is stabilized with lengthening alkoxy chain.

One of the main objects of the present studies was to construct a 'phase diagram' within the Cub phase region, and the phase types determined by XRD measurements (the details of which are mentioned and discussed below) are already shown in figure 1. The result reveals the presence of two types of Cub phase in the region, one with $Im3m$ (and denoted Cub I in this paper) and the other with $Ia3d$ symmetry (Cub II). A noteworthy feature of the Cub phase region is that the $Im3m$ Cub phase region intervenes between two regions of $Ia3d$ Cub phase; the homologues $n = 15$, 16, 17, and 18 exhibit an $Ia3d$ Cub phase, in agreement with previous reports for $n = 16$ [8] and 18 [16, 21], whereas those of $n = 19$, 20, and 21 exhibit an $Im3m$ Cub phase, and for $n = 22$ and 26, the $Ia3d$ type was again observed in their high temperature region.

The XRD patterns of the various ANBC-n homologues in the Cub I phase are presented in figure 2 and the patterns in the Cub II phase are shown in figure 3. Here, the abscissa q is defined as $q = (4\pi/\lambda) \sin\theta$, with

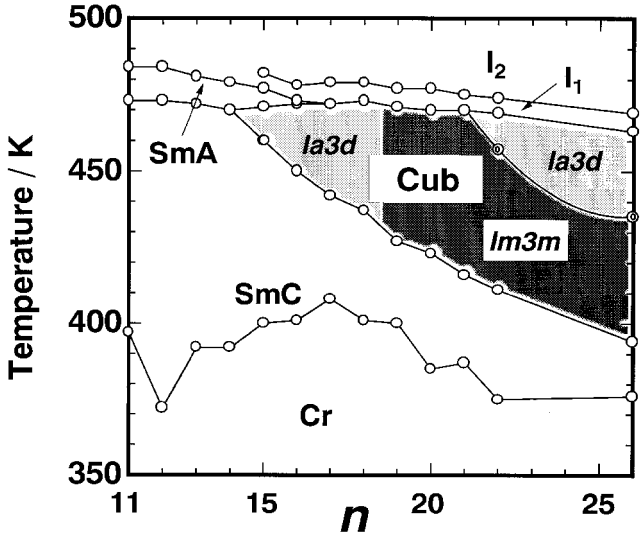

Figure 1. Phase diagram for ANBC-n (Cr, crystal; SmC/A, smectic C/A; Cub, cubic; I_1, I_2, isotropic liquid phases). The space group of the Cub phases, determined by XRD measurements, is also shown.

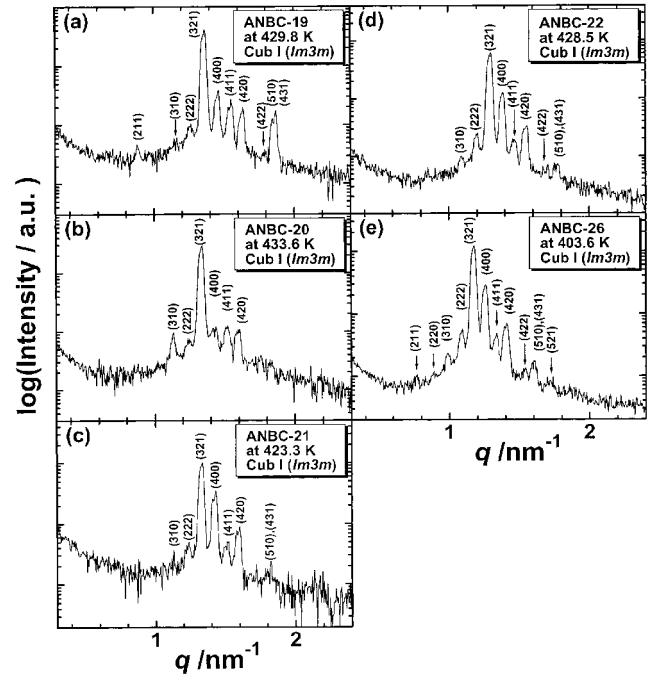

Figure 2. XRD patterns of the $Im3m$ Cub (Cub I) phases of various ANBC-n homologues. The pattern was detected by PSPC and Miller indices are shown in the figure.

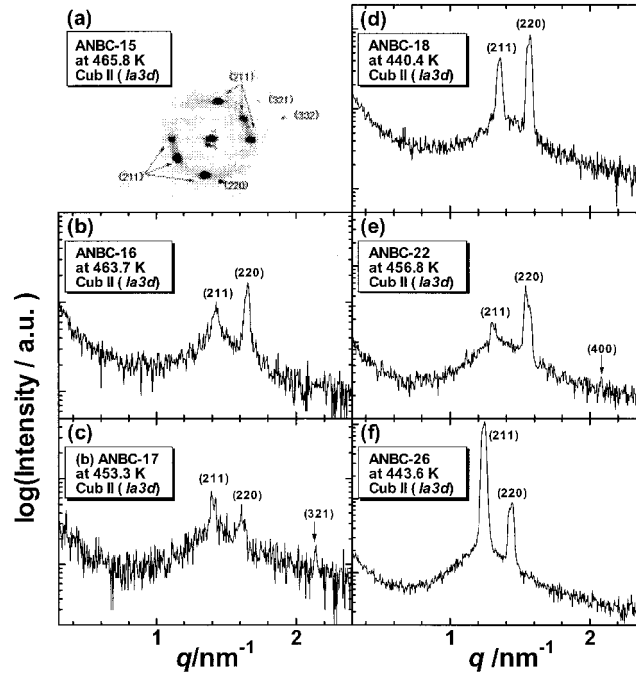

Figure 3. XRD patterns of the $Ia3d$ Cub (Cub II) phases of various ANBC-n homologues. The pattern in (*a*) was recorded on IP and those in (*b*)–(*f*) were detected by PSPC; Miller indices are also shown in the figure.

$\lambda = 0.154$ nm and $\theta =$ the scattering angle. The Cub I phase exhibits 6 to 11 diffraction peaks the Miller indices of which $(h\,k\,l)$ all satisfy $h+k+l=2n$ ($n=$ integer). 6 space groups of cubic systems match this condition and the most symmetric case is the space group $Im3m$. Thus, the phase is most probably identified as having the space group $Im3m$. For the Cub II phase, on the other hand, the number of diffraction peaks detected by one-dimensional PSPC was usually very small and sometimes only one or two peaks were seen, which made it a problem to determine the space group unambiguously. As shown in figure 3(*a*), in the two-dimensional IP image, the patterns of the Cub II phase often became spot-like because of the easy growth of fairly large domains [5, 7]. This tendency was significant for the homologues with smaller n such as $n=15$ and 16. However, careful duplicate measurements using both PSPC and IP, and running the samples to a given temperature through a relatively rapid heating or cooling process, led us to the conclusion that the diffractions with lower indices (1 0 0), (1 1 0), (1 1 1), (2 0 0) and (2 1 0) are always absent for the Cub II phase, and two space groups $I43d$ and $Ia3d$ match the condition. Since the space group $Ia3d$ is frequently adopted in the literature for lyotropic cubic systems [2, 35], $Ia3d$ is selected for the Cub II phase. In fact, higher indices (2 1 1), (2 2 0), (3 2 1), (4 0 0), (4 2 0) and (3 3 2), which are observable for both $Ia3d$ and $I43d$, were observed, but for example, the diffraction (3 1 0), observable only for $I43d$, was not.

Figure 4 summarizes the plots of d-spacing versus temperature T for all ANBC-n examined except $n=18$. In the figure, open and filled symbols represent the data on heating and cooling, respectively. Four points are noted:

(1) The slopes of the d versus T plots are all slightly negative. This means for the SmC phase, a thinning of the SmC layer thickness with increasing T, and for the Cub region, a contraction of the unit lattice with T. In a separate experiment, for ANBC-22, the specific volume was found to increase with increasing T in both the Cub I and II regions [36]. Therefore, the number of molecules forming a cubic unit lattice is not constant and decreases with increasing T. We shall call this the *fluid nature* of the Cub phases, in that it is similar to the number of liquid water molecules in a unit volume which varies with temperature, and it definitely distinguishes them from disordered crystals. The table summarizes the apparent thermal volume expansion coefficient α of the Cub phases of the ANBC-n homologues; this was estimated by using the relation $\alpha=(1/a^3)\,(\partial a^3/\partial T)$, where a is the cubic lattice constant. Here, 'apparent' implies that such a definition is not strictly allowed from a thermodynamic point of view.

(2) For $n=15$–17, the variation of the SmC layer spacing with T is roughly linear and seems continuous with the temperature variation of the Cub II (2 1 1) spacing across the phase boundary. This suggests the existence of an epitaxial relationship between the two phases, very similar to the case of lyotropic cubic systems at the lamellar to

Table 1. Apparent thermal volume expansion coefficients α (in K^{-1}), determined by XRD[a], of the Cub phases of ANBC-n.

n		$Im3m$ Cub phase	$Ia3d$ Cub phase
16	heating	—	-7×10^{-4} (451–471 K)[b]
	cooling	—	no data
17	heating	—	-1.3×10^{-3} (442–469 K)
	cooling	—	-1.4×10^{-3} (424–463 K)
18	heating	—	-1.0×10^{-3} (434–469 K)
	cooling	—	-1.4×10^{-3} (409–464 K)
19	heating	-4×10^{-5} (426–467 K)	—
	cooling	-3×10^{-4} (403–463 K)	—
20	heating	-9×10^{-4} (421–469 K)	—
	cooling	-9×10^{-4} (391–465 K)	—
21	heating	-9×10^{-4} (414–469 K)	—
	cooling	-7×10^{-4} (382–463 K)	—
22	heating	-1.3×10^{-3} (411–454 K)	-6×10^{-4} (454–469 K)
	cooling	—	-3×10^{-4} (385–464 K)
26	heating	-2.3×10^{-3} (395–428 K)	-7×10^{-4} (428–467 K)
	cooling	—	-8×10^{-4} (366–462 K)

[a] $\alpha=(1/a^3)\,(\partial a^3/\partial T)$, where a is the cubic lattice constant.
[b] Temperature region of each phase in parenthesis.

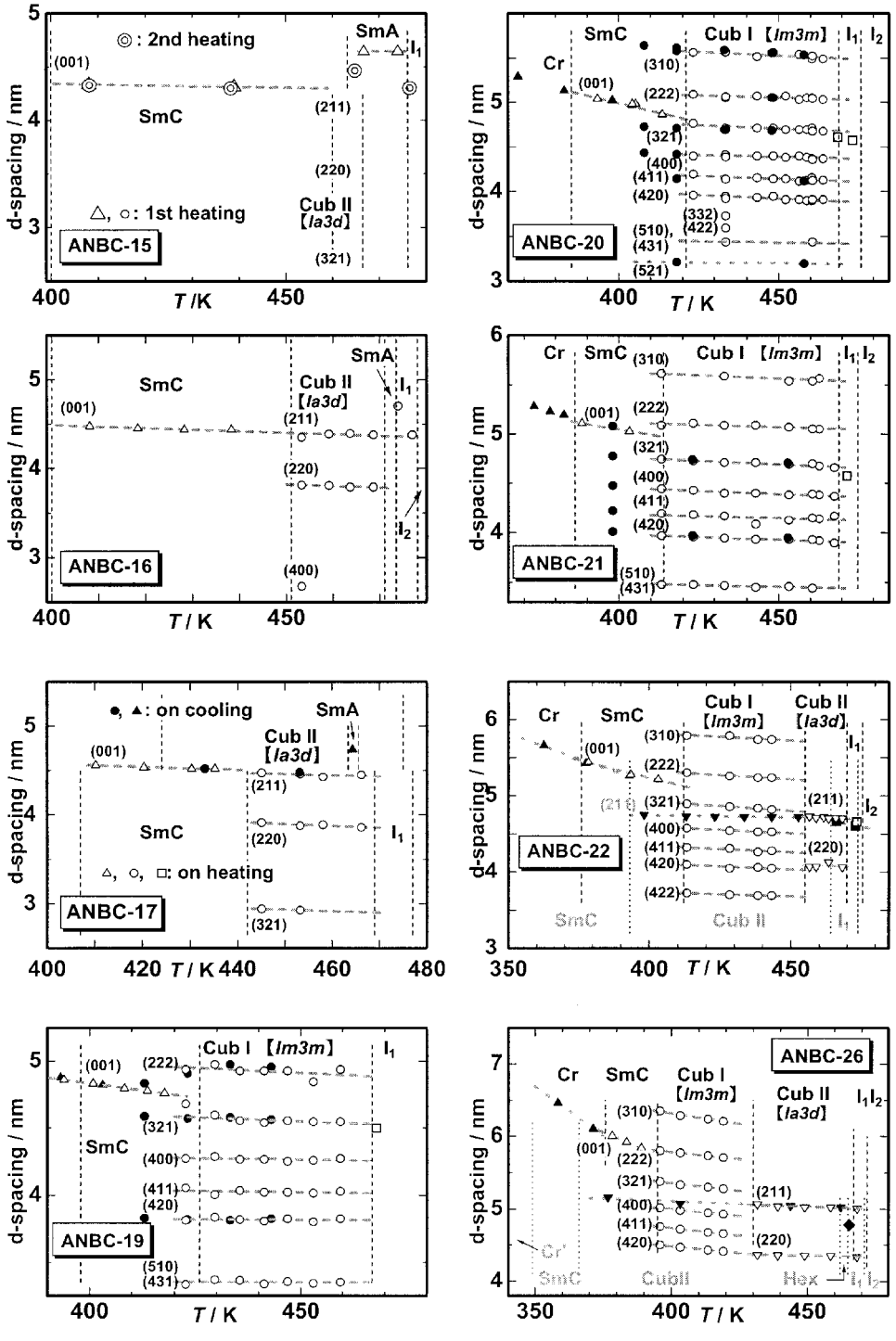

Figure 4. Plots of d-spacing versus temperature (T) for all ANBC-n examined except $n = 18$; open and filled symbols represent the data on heating and cooling, respectively.

$Ia3d$ Cub phase transition [37]. For $n = 19$–21, the SmC layer spacing seems to change into the spacing of the Cub I (3 2 1) phase with a small discontinuity on heating. The (3 2 1) plane was the highest density plane of the Cub I phase. On cooling, however, the Cub I (2 2 2) spacing seems to change continuously into the SmC spacing across the phase boundary. For $n = 22$ and 26, the highest density plane changes from the SmC layer plane to the Cub I (3 2 1) plane and to the

Cub II (2 1 1) plane with small discontinuities at the phase transitions. To obtain definite conclusions, however, further detailed experiments are necessary using oriented samples.

(3) Reversibility: For $n = 17$ and 19–21, the d versus T plot in the Cub temperature region on cooling (filled circles) is completely superposed on the plot for heating (open circles), except that the region becomes extended on the lower temperature side owing to supercooling. Thus, the type of Cub phase is the same both on heating and cooling for these homologues. For $n = 22$ and 26, on the other hand, two types of Cub phase are present on heating, the Cub I phase with $Im3m$ symmetry in the low temperature region and the Cub II phase with $Ia3d$ symmetry in the high temperature region. On cooling, only the Cub II phase is observed, the Cub I phase being absent. Probably, the formation of the $Im3m$ Cub phase is strongly affected by the preceding phase structure on the thermal cycle used for $n = 22$ and 26. There have been reports about similar observations [23, 38, 39].

(4) For $n = 26$, a hexagonal columnar (Hex) phase appears with a temperature interval of only 2 K on cooling. This phase was detected by both POM and XRD [28]. Regarding this, it has been reported that a metastable S_4 [9–11] or a tetragonal [21] phase is frequently observed for the shorter alkoxy ANBC-n such as $n = 16$ and $n = 18$ especially by POM before the change into the Cub phase on cooling. The existence of this, however, was not detected by the present XRD studies.

In our previous publication [27], the cubic phases of $n = 19$ and 20 were assigned to the space group $Ia3d$ and the same assignment was made to the cubic phase for $n = 22$ at 433 K. These assignments have been corrected by the present XRD characterization by using a high resolution SAXS apparatus.

Figure 4 does not include the data on ANBC-18; these are shown separately in figure 5. Crudely speaking, in the d-spacing versus T plots, the $Ia3d$ type Cub II phase was observed both on heating and cooling, as reported by other researchers [16, 21], and an epitaxial relation is obtained between the SmC layer spacing and the Cub II (2 1 1) spacing at the phase boundary, as seen for $n = 15$–17 in figure 4. Very surprisingly, as shown in the pattern in the upper part of figure 5, the 'coexistence' of another series of diffraction peaks of the $Im3m$ type was very often observed in the high temperature region above ≈ 450 K on heating. These are plotted with the symbol $\diamond$ in the plots in the lower part of the figure. It is not certain at this stage whether this observation really indicates the coexistence of two Cub phases at the

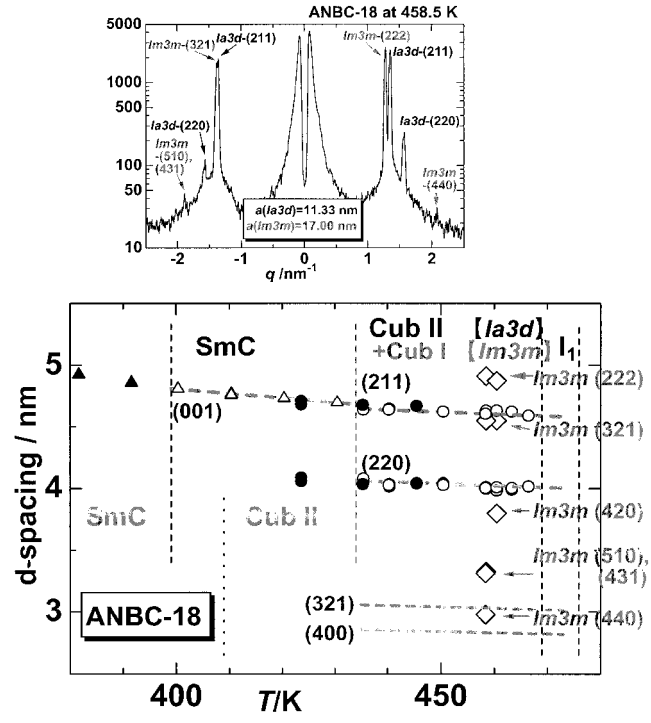

Figure 5. (Top) XRD pattern of ANBC-18 recorded at 458.5 K in the Cub phase region on heating; two Cub lattices are present and their Miller indices are shown in the figure. (Bottom) Plots of d-spacing versus temperature (T) for ANBC-18, where open and filled symbols represent the data on heating and cooling, respectively.

same time or else a structural fluctuation between the two phases with time, because the presence of small air bubbles in the capillary tubes changes the sample position being irradiated slightly from time to time during the measurement, causing a change in the total intensity with time. Since this is a pure one-component system, it is not easy to accept the coexistence of two Cub phases because it is not thermodynamically allowed. Thus, a structural fluctuation between the two is more likely. This unusual observation was confirmed in triplicate experiments for $n = 18$, but never found for ANBC homologues other than $n = 18$.

Figure 6 shows the temperature dependence of the storage modulus (G') and loss modulus (G'') at 62.8 rad s^{-1} for ANBC-18 in the Cub temperature region on heating. As observed for other ANBC-n homologues in the Cub phase [18, 23], the G' value is around 10^7 dyn cm^{-2} (1 dyn $cm^{-2} = 0.1$ Pa), much higher than the usual values for smectic phases (10^3–10^4 dyn cm^{-2}). It is clear that the high value of G' reflects the three-dimensionally isotropic organization of this phase; smectic phases can flow through a slippage of layers without a breakdown of the structure, whereas the three-dimensional network structure of the Cub phases could offer resistance to the shear distortion. A significant fact not seen

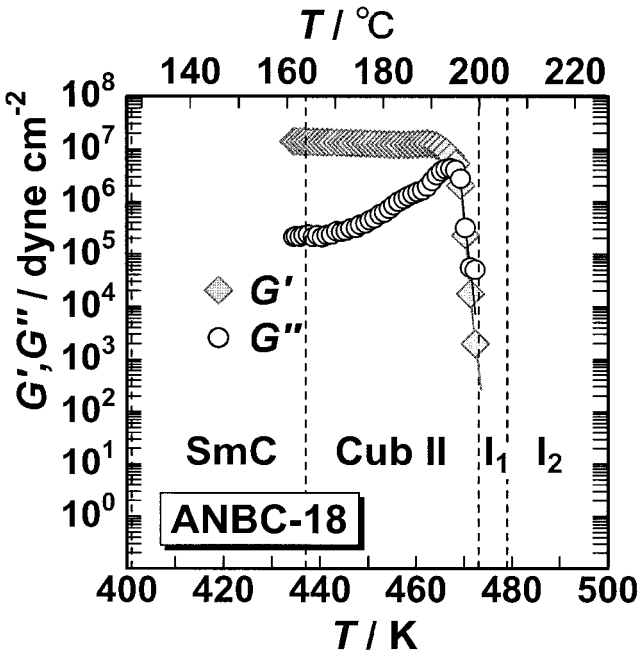

Figure 6. Temperature dependence of the storage modulus (G') and loss modulus (G'') at 62.8 rad s^{-1} for ANBC-18 in the Cub temperature region on heating (heating rate: 1 K min^{-1}).

for other homologues in the Cub phase is that the G'' value, which is constant with temperature below $\approx$ 450 K, steeply increases above this temperature, suggestive of the existence of a *structural relaxation*. This fact is probably related to the unusual XRD observation mentioned above, and so it is concluded that the $Ia3d$ Cub structure of ANBC-18 is severely subject to thermal fluctuations above $\approx$ 450 K, resulting in the transformation between the $Ia3d$ Cub and $Im3m$ Cub structures. As discussed later, a reason why this happens only for ANBC-18 may arise from the close proximity of the Gibbs free energy versus temperature curves for the two Cub phases.

4. Discussion

4.1. *Gibbs free energy versus temperature curves for the two Cub phases*

Professors Sorai and Saito and their colleagues have precisely measured heat capacities of the ANBC-n homologues with different chain lengths $n = 16$, 18 and 22 by adiabatic calorimetry, and the excess entropy acquisition with temperature was determined [22, 24, 29, 30]. The sequence of SmC, $Im3m$ Cub, and $Ia3d$ Cub phases was deduced from an analysis of the chain length dependence of the SmC to Cub transition entropy ($\Delta S_{\mathrm{SmC\text{-}Cub}}$). They also postulated the 'alkyl chains as entropy reservoir' mechanism for the SmC to Cub phase transition; the contributions of the core and the alkyl chain to the transition entropy have opposite signs and the entropy is virtually transferred from the core to the alkyl chain.

On the basis of their interpretation, the present XRD characterization of the Cub phases has enabled us to depict the G versus T curves as diagrams for various chain lengths n, where the slope of the G–T curve corresponds to the entropy of the phase. Figure 7 schematically illustrates the G–T curves for the SmC, $Im3m$ Cub, $Ia3d$ Cub, and isotropic liquid (I) phases. The G–T curve for the SmA phase of $n = 16$ and the distinction between the I_1 (a structured liquid) and I_2 (the true isotropic liquid) phases are neglected for clarity. An important point is that the dependence of the Cub phase type on n and T (figure 1), which seems complicated at first sight, is thermodynamically allowed by postulating different dependences on n of the G–T curves for the two Cub phases; as depicted in (f) and (g), the n dependence of the slope of the G–T curve for the $Ia3d$ Cub phase would

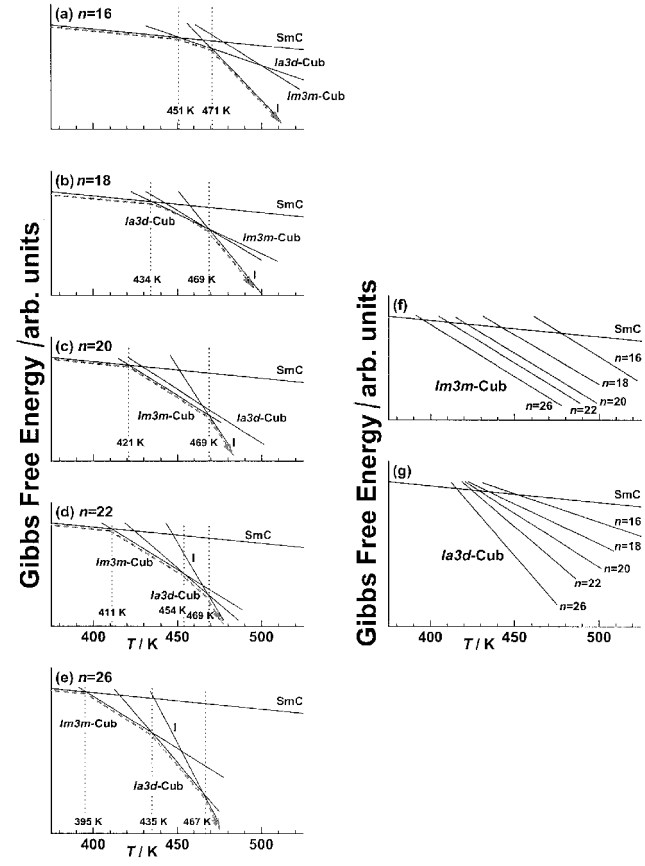

Figure 7. Schematic Gibbs free energy (G) versus temperature (T) curves for the SmC, $Im3m$ Cub, $Ia3d$ Cub, and isotropic liquid (I) phases of various ANBC-n. The G–T curve for the SmA phase of $n = 16$ and the distinction between the I_1 and I_2 phases are neglected for clarity in this figure. In (f) and (g), the n dependence of the G–T curve for the $Im3m$ Cub phase and that for the $Ia3d$ Cub phase are shown, respectively.

be larger than that for the $Im3m$ Cub phase. To confirm this postulate further, calorimetric measurements for $n=20$ are currently in progress.

Another feature of the G–T diagrams is that for $n=18$ the G–T curves for the two Cub phases can be very close to each other in the high temperature region of the Cub phase. Therefore, the observation of the 'coexistence' of the two Cub phases (figure 5) may be qualitatively understood by considering the proximity of the two G–T curves and the resulting thermal fluctuations between the two states.

In conjunction with the Cub phase of ANBC-18, Levelut and Fang [16] and Levelut and Clerc [21] identified the Cub phase of the $n=18$ cyano analogue, 4′-n-octadecyloxy-3′-cyanobiphenyl-4-carboxylic acid (often denoted as ACBC-18), as having the space group $Im3m$. Initially, these reports confused us, because the space group of the Cub phase seemed to be entirely $Im3m$ for the ACBC-n homologues and very sensitive to the type of the side group at the 3′ position of the biphenyl core, i.e. CN or NO_2. The phase diagram of figure 1, however, shows that the cubic phase of ANBC-19 is of $Im3m$ type and thus, the $Im3m$ type of ACBC-18 is now not so surprising.

4.2. *Temperature dependence of the SmC layer spacing for various ANBC-n homologues*

Figure 8 shows the temperature dependence of the SmC layer spacing for various ANBC-n homologues on heating. When the temperature T is raised, the SmC phase of $n \geqq 15$ undergoes a transition to a Cub phase with $Ia3d$ or $Im3m$ symmetry, whereas that of $n=14$ is transformed into the SmA phase. In figure 8, for all n except $n=14$, the layer spacing (L_{SmC}) decreases almost linearly with increasing T. The thinning of the SmC layer with increase of T is characteristic of the phase when it exhibits any Cub phase on the higher temperature side (at least for ANBC-n homologues).

The negative slope dL_{SmC}/dT varies with n, and is presented in figure 9, together with the plots of the SmC layer thickness at the SmC to Cub transition temperature ($T_{SmC\text{-}Cub}$) as a function of n. As n increases from $n=15$, the dL_{SmC}/dT value initially slowly decreases, but beyond $n=18$ decreases strongly showing a strong odd–even alternation. The type of the Cub phase neighboured by the SmC phase is changed from $Ia3d$ to $Im3m$ beyond $n=18$. On the other hand, the SmC layer thickness at $T_{SmC\text{-}Cub}$ increases with increasing n, but the increment with n changes between $n \leqq 18$ and $n \geqq 19$, which also corresponds with the cubic type neighboured by the SmC phase. The linear least-squares fits gave a relation of $L_{SmC}=2.46+0.122n$ for $n \leqq 18$ and $L_{SmC}=1.87+0.148n$ for $n \geqq 19$.

It may be said that the intercept at $n=0$ corresponds to the effective core size, which is different between $n \leqq 18$ and $n \geqq 19$. The effective core size was deduced to be 2.46 nm for the shorter alkoxy ANBC-n and 1.87 nm for the longer alkoxy homologues, while the

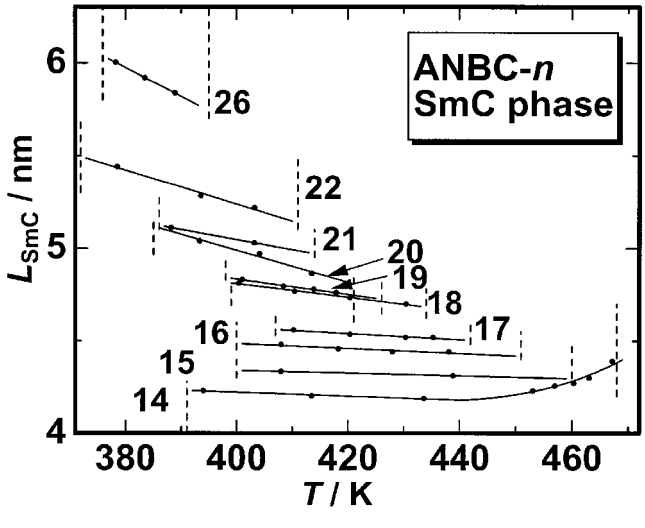

Figure 8. Temperature dependence of the SmC layer spacing (L_{SmC}) for various ANBC-n homologues on heating.

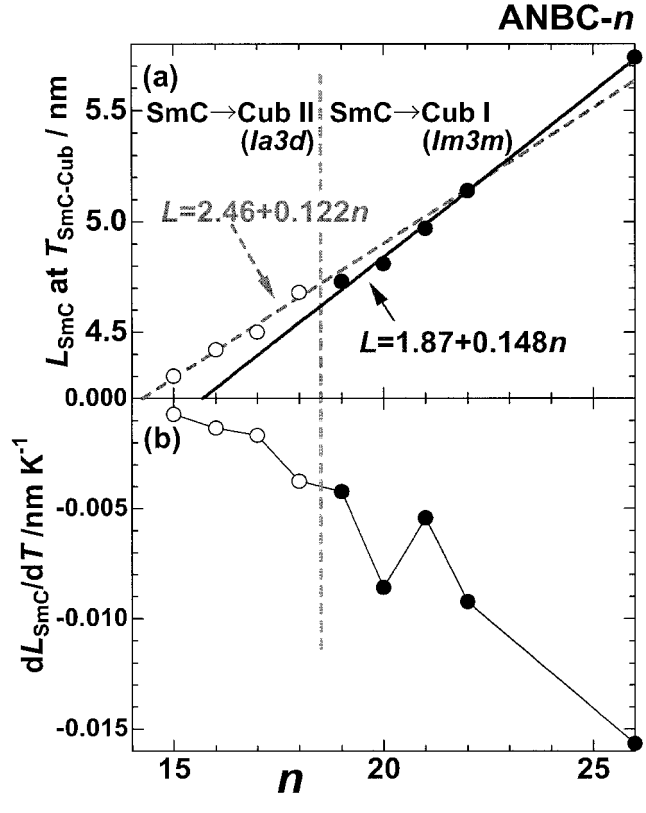

Figure 9. (*a*) Plots of the SmC layer spacing (L_{SmC}) just below the SmC to Cub transition temperature ($T_{SmC\text{-}Cub}$); and (*b*) of the variation of L_{SmC} with temperature (T) (dL_{SmC}/dT), as functions of the alkoxy chain length n.

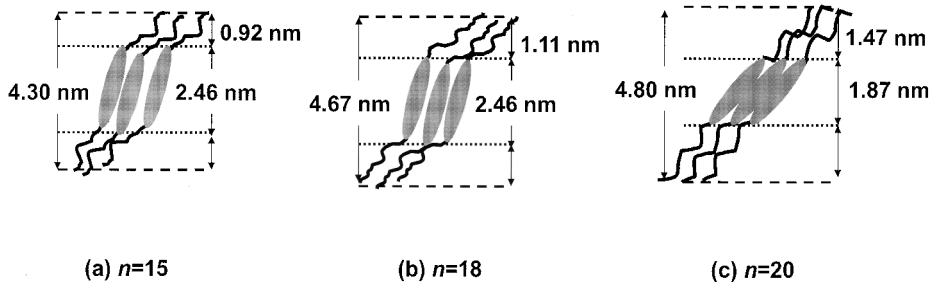

Figure 10. Schematic diagrams of the molecular organizations in the SmC phase for (a) ANBC-15, (b) ANBC-18 and (c) ANBC-20.

core size estimated by using Chem 3D software was 2.4 nm. Furthermore, the tilt angle β in the SmC phase could be estimated using the relation $\cos\beta = L_{SmC}/L_{SmA}$, where L_{SmA} is the layer thickness of the SmA phase. The β values lay between 16° and 23° for $n = 14$–17.

On the basis of these results, the molecular organization in the SmC phase is schematically depicted in figure 10. Although the structural model is probably oversimplified, one feature is noted: for the homologues whose SmC phase is transformed into the $Ia3d$ type Cub II phase at a higher temperature, the core is only slightly tilted with respect to the layer normal in the SmC phase, whereas for those into the $Im3m$ type Cub I phase, the core is strongly tilted. This probably reflects the fact that in the SmC phase the core–core interaction is stronger in the longer alkoxy homologues than in the shorter ones, as a consequence of the larger deviation from 1 of the volume ratio of the aliphatic tail to aromatic core part, a factor which seems to be closely connected to the molecular organizations in the two Cub phases on the high temperature side.

4.3. *Lattice parameter versus alkoxy chain length for the two Cub phases*

Figure 11 shows plots of the cubic lattice constant a versus alkoxy chain length n for the two Cub phases. The a value of the $Im3m$ Cub phase increases almost linearly with n, with the relation $a = 9.8 + 0.38n$. For the $Ia3d$ Cub phase, on the other hand, the dependence of the a value on n is divided into two straight lines, $a = 5.7 + 0.32n$ for $15 \leqq n \leqq 18$ and $a = 7.3 + 0.19n$ for $22 \leqq n \leqq 26$; we could find no relation for the whole n region.

For the $Ia3d$ Cub phase, the most accepted structure is a bicontinuous type. Luzzati and Spegt postulated a skeletal structure for the $Ia3d$ Cub phase (labelled Q phase) of anhydrous strontium soaps, which shows that rod-like micelles are joined 3-by-3 to form two sets of interwoven networks [35]. An alternative description is the infinite periodic minimal surface (IPMS) model and the G-surface corresponds to the $Ia3d$ Cub structure

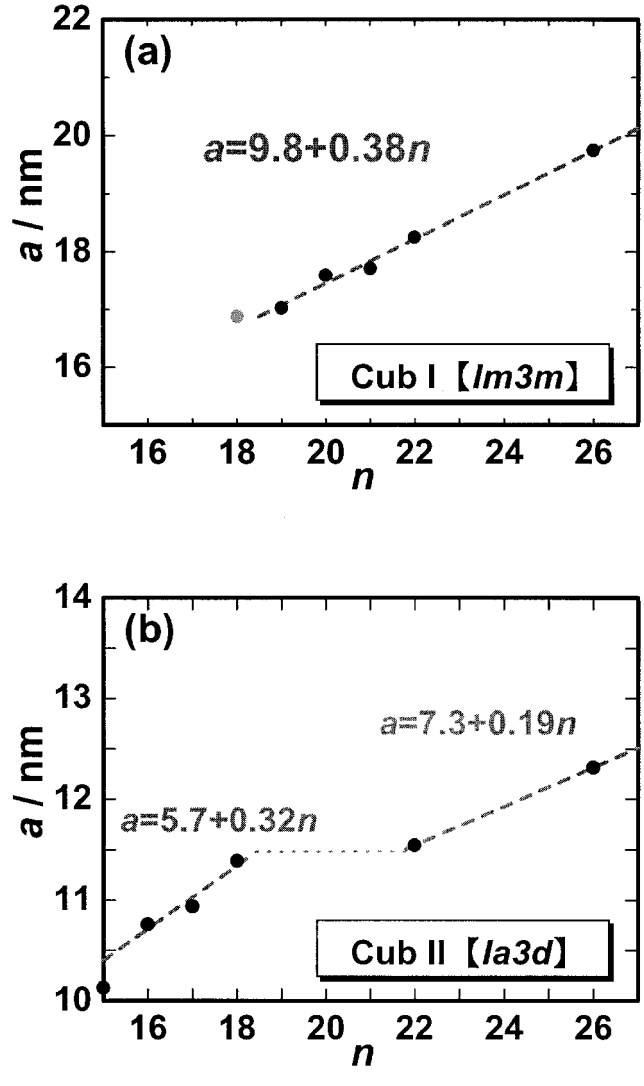

Figure 11. Plots of the cubic lattice constant a versus alkoxy chain length n for the two Cub phases, where straight lines represent least-squares fits for the data. The a value for the $Im3m$ Cub I phase was calculated from the data at ≈425 K and that for the $Ia3d$ Cub II phase from the data at ≈455 K, but the temperatures were not exactly the same, depending on the phase region.

[40–42]. The molecular structure of anhydrous strontium soaps consists of the strontium carboxylate core ($^{-}COO^{-}Sr^{2+}{}^{-}OOC^{-}$) and alkyl chains at both ends. It is generally considered that the core part forms the 'skeletons' in the skeletal graph and the alkyl chain fills the remaining space between the skeletons; in the IPMS description, correspondingly, the methyl end groups form the G-surface. This picture, however, is not so certain as the bicontinuous structure, and the reverse picture, i.e. with the methyl end group of the chain on the skeletons, may be possible [43].

For ANBC-n, the basic units constructing the cubic structure are hydrogen-bonded ANBC-n dimers [19], in which the aromatic part and the dimeric COOH groups act as the core with long alkoxy chains at both ends, similarly to the strontium soaps. In fact, the increment in the lattice constant a with respect to the alkoxy chain length n for $15 \leqq n \leqq 18$ is almost the same in the case of the anhydrous strontium soaps ($a = 7.5 + 0.35n$ for $n = 12, 14, 16, 18, 20, 22$) [35]. The diameter of the rod-like micelles is approximately estimated as $D = (a\sqrt{5})/8$ by calculating the distance between two adjacent but not connecting rods [27, 35]. Here, note that D is not the diameter of the 'skeleton' in the skeletal graph. For $n \geqq 15$, the D are 5–35% less than the length of the ANBC-n dimer in the extended form. This indicates that in the $Ia3d$ Cub phase, D corresponds to the length of *one* dimer with substantially curled alkoxy chains.

For $22 \leqq n \leqq 26$, in addition to the $Ia3d$ Cub phase, the ANBC-n exhibit the $Im3m$ Cub phase on the low temperature side on heating, and the increment of a for the $Ia3d$ Cub phase with n is much diminished compared with the region $15 \leqq n \leqq 18$. Moreover, the a value for $n = 22$ is very close to that of $n = 18$, which implies a decreased number of molecules constructing a unit lattice, reflecting the decreased curvature in the G-surface. Here, we simply consider the ratio of a to the molecular length (or n) as a measure of the curvature. We have attributed this behaviour to weakening of the hydrogen-bonded COOH linkage in the ANBC-n core part. According to the packing considerations first postulated by Israelachvili for lyotropic systems [44], the average shape of the building unit plays a key role in forming a variety of aggregation structures, and if the average shape is regarded as cylinder-like, a flat layer structure is constructed, but the deformation from a cylinder to a truncated cone results in a strong curvature of the layer structure, giving rise to a rod-like micelle, and as an intermediate aggregation state, cubic mesophases are realized. In the ANBC-n, it is reasonable to consider that two competing factors, the extension in space of the alkyl tails vs the effective volume of the ANBC-n core part containing the hydrogen-bonded COOH linkage, determines the average shape of the building unit. As expected, the former factor is enhanced when the temperature is raised or the length of the alkyl chain is increased, so deforming the ANBC-n dimers to a shape like two truncated cones with the two tops joined, where cubic mesophases are favoured. In the case of the latter factor, on the other hand, weakening of the hydrogen bonding caused by raising temperature would contribute to putting the deformation slightly back towards a cylindrical shape and to reducing the curvature of the layer. For $n = 22$ and 26, the aggregation interaction between the core parts in the temperature region of the $Ia3d$ Cub phase would become weaker than in the $Im3m$ Cub region. The dynamic viscoelastic measurement for ANBC-22 gave a result supporting this consideration; in the temperature region of the $Im3m$ Cub phase, the storage modulus (G') is one magnitude larger than the loss modulus (G'') at 6.28 rad s^{-1}, whereas the values of both are almost the same in the $Ia3d$ Cub region, reflecting the closer nature to a true liquid compared with the $Im3m$ Cub phase [18, 23]. In the schematic G–T diagram in figure 7, this is represented by the fact that the slope of the G–T curve (and thus, the entropy) of the $Ia3d$ Cub state is larger than that of the $Im3m$ Cub state.

The structure of the $Im3m$ Cub phase is mysterious. Luzzati and coworker proposed a structure of lyotropic Cub phases with $Im3m$ symmetry using a skeletal graph, where the skeletons forming the networks are joined not 3-by-3 but 6-by-6, so that they are directed parallel to one of three lattice axes [2]. The problem of applying this structure to the $Im3m$ Cub phase of the ANBC-n arises from the fact that the diameter of the rod-like micelles corresponds to the length of two ANBC-n dimers or more [28]. In the lyotropic $Im3m$ Cub phases, the (1 1 0) diffraction peak is the most intensely observed [2], which is readily understood on the basis of Luzzati's skeletal graph. For the $Im3m$ Cub phase of the ANBC-n, however, the most intense plane is (3 2 1) as seen in figure 2, which suggests that the structure is less simple than Luzzati's model.

In the IPMS description, the P-surface describes the $Im3m$ Cub structure [40–42]. For the $Im3m$ Cub phase of an ANBC-n analogue, i.e. ACBC-18, a modified version of the P-surface has been proposed using a space foliation; the Cub phase contains three continuous surfaces [21]. The total surface area per unit lattice S is given by $S = 5.39a^2$ [21], where a is the lattice constant. In the case of an $Ia3d$ cubic IPMS of type G, the corresponding relation is $S = 3.091a^2$ [43]. Provided that the surface of area S is covered by the methyl end groups on both sides, the alkyl chain area A, reflecting the thermal motion of the methyl end group, is defined as $A = S/(N_0/2)$; and N_0, the number of methyl groups in the unit lattice, is given by $(\rho a^3)/(M/N_A)$, where ρ is

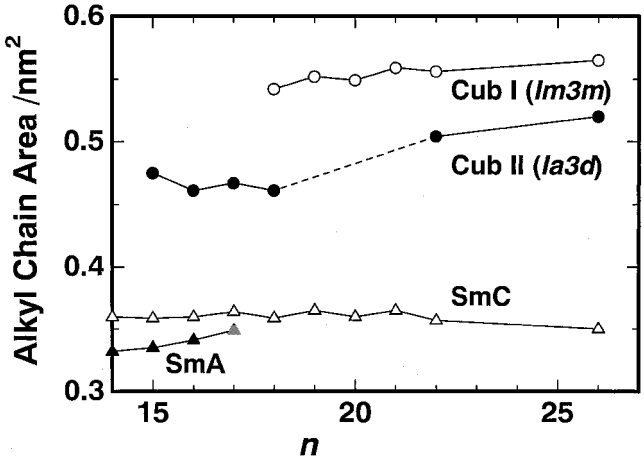

Figure 12. Plots of alkyl chain area A as functions of the phase type and the alkoxy chain length n on heating, except the grey triangle which is for the SmA phase of $n = 17$ on cooling.

the density, assumed to be 1 g cm^{-3}, M is the molecular mass, and N_A is Avogadro's number. On the other hand, the A value for a flat layer structure with thickness L ($= L_{SmA}$ or L_{SmC}) can be calculated using the relation $N_0 = (\rho LS)/(M/N_A)$, where N_0 is the number of methyl groups in the volume LS. Assuming that the space-foliated P-surface model (at least) approximately describes the real structure of the $Im3m$ Cub phase, we can calculate how the alkyl chain area A depends on the phase type and the alkoxy chain length n, as is shown in figure 12. Although the value of A is expected to increase with increasing temperature, the phase sequences SmC $\rightarrow$ $Ia3d$ Cub $\rightarrow$ SmA on heating for $n = 15$ and 16, and SmC $\rightarrow$ $Im3m$ Cub $\rightarrow$ $Ia3d$ Cub for $n = 22$ and 26, are not necessarily consistent with an increase of A [45].† This clearly implies that this parameter is not the only one governing the phase behaviour in thermotropic liquid crystalline systems exhibiting Cub phases such as the ANBC-n homologues.

We thank Dr Satoshi Tanimoto at JAIST for his kind help with the X-ray experiment using IP. We are grateful to Prof. Michio Sorai and Kazuya Saito at Osaka University for the collaborative work on heat capacity of ANBC-22 and valuable discussions, and to Prof. Keiichi Moriya at Gifu University for his valuable experimental suggestions. Thanks are also due to Ms Yumiko Murase and Eri Kumita at the Instrumental Analysis Center, Gifu University, for the measurements of MS spectra. This work was supported by Grant-in-Aid for Scientific Research on Priority Areas (A), 'Dynamic Control of Strongly Correlated Soft Materials' (No. 413/13031037) from the Ministry of Education, Science, Sports, Culture, and Technology in Japan, and partly supported by the Research Foundation for Electrotechnology of Chubu (R-11123) and the Saneyoshi Foundation (No. 1343).

†After submitting the manuscript, we learned of this report, which shows $S = 4.10a^2$ for the 'double' structure of type P, where the simple P layer is made up of bilayers and so the unit cell contains two continuous surfaces. If we use the model of [45], the value of S lies in the range 0.41–0.43 nm^2 and seems to show an intermediate value between those for SmC and $Ia3d$ Cub phases.

References

[1] Diele, S., and Göring, P., 1998, *Handbook of Liquid Crystals*, Vol 2B, edited by D. Demus, J. Goodby, G. W. Gray, H.-W. Spiess, and V. Vill (Weinheim: Wiley-VCH), pp. 887–900.
[2] Mariani, P., Luzzati, V., and Delacroix, H., 1988, *J. mol. Biol.*, **204,** 165.
[3] Bates, F. S., and Fredrickson, G. H., 1990, *Ann. Rev. phys. Chem.*, **41,** 525.
[4] Gray, G. W., Jones, B., and Marson, F., 1957, *J. chem. Soc.*, 393.
[5] Demus, D., Kunicke, G., Neelsen, J., and Sackmann, H., 1968, *Z. Naturforsch.*, **23a,** 84.
[6] Pelzl, G., and Sackmann, H., 1971, *Symp. chem. Soc., Faraday Div.*, **5,** 68.
[7] Diele, S., Brand, P., and Sackmann, H., 1972, *Mol. Cryst. liq. Cryst.*, **17,** 163.
[8] Tardieu, A., and Billard, J., 1976, *J. Phys. (Paris) Coll.*, **37,** C3-79.
[9] Demus, D., Marzotko, D., Sharma, N. K., and Wiegeleben, A., 1980, *Krist. Tech.*, **15,** 331.
[10] Gray, G. W., and Goodby, J. W., 1984, *Smectic Liquid Crystals* (Glasgow: Leonard Hill), pp. 68–81, including earlier references on thermotropic cubic phases.
[11] Gray, G. W., 1986, *Zehn Arbeiten uber Flüssige Kristalle, Kongress-und Tagung-berichte der Martin-Luther-Universität, Halle-Wittenberg*, pp. 22–42.
[12] Etherington, G., Leadbetter, A. J., Wang, X. J., Gray, G. W., and Tajbakhsh, A., 1986, *Liq. Cryst.*, **1,** 209.
[13] Ukleja, P., Siatkowski, R. E., and Neubert, M. E., 1988, *Phys. Rev. A*, **38,** 4815.
[14] Etherington, G., Langley, A. J., Leadbetter, A. J., and Wang, X. J., 1988, *Liq. Cryst.*, **3,** 155.
[15] Billard, J., Zimmermann, H., Poupko, R., and Luz, Z., 1989, *J. Phys. (Paris)*, **50,** 539, including references on other types of thermotropic cubic phases.
[16] Levelut, A.-M., and Fang, Y., 1990, *Coll. Phys., Coll.*, **51,** C7-229.
[17] Kutsumizu, S., Yamada, M., and Yano, S., 1994, *Liq. Cryst.*, **16,** 1109.
[18] Yamaguchi, T., Yamada, M., Kutsumizu, S., and Yano, S., 1995, *Chem. Phys. Lett.*, **240,** 105.
[19] Kutsumizu, S., Kato, R., Yamada, M., and Yano, S., 1997, *J. phys. Chem. B*, **101,** 10 666.
[20] Tansho, M., Onoda, Y., Kato, R., Kutsumizu, S., and Yano, S., 1998, *Liq. Cryst.*, **24,** 525.
[21] Levelut, A.-M., and Clerc, M., 1998, *Liq. Cryst.*, **24,** 105.
[22] Sato, A., Saito, K., and Sorai, M., 1999, *Liq. Cryst.*, **26,** 341.

[23] KUTSUMIZU, S., YAMAGUCHI, T., KATO, R., and YANO, S., 1999, *Liq. Cryst.*, **26,** 567.
[24] SATO, A., YAMAMURA, Y., SAITO, K., and SORAI, M., 1999, *Liq. Cryst.*, **26,** 1185.
[25] KUTSUMIZU, S., ICHIKAWA, T., NOJIMA, S., and YANO, S., 1999, *Chem. Commun.*, 1181.
[26] KUTSUMIZU, S., YAMAGUCHI, T., KATO, R., ICHIKAWA, T., and YANO, S., 1999, *Mol. Cryst. liq. Cryst.*, **330,** 359.
[27] KUTSUMIZU, S., KOBAYASHI, H., NAKAMURA, N., ICHIKAWA, T., YANO, S., and NOJIMA, S., 2000, *Mol. Cryst. liq. Cryst.*, **347,** 239.
[28] KUTSUMIZU, S., ICHIKAWA, T., YAMADA, M., NOJIMA, S., and YANO, S., 2000, *J. phys. Chem. B*, **44,** 10 196.
[29] SAITO, K., SHINHARA, T., and SORAI, M., 2000, *Liq. Cryst.*, **27,** 1555.
[30] SAITO, K., SHINHARA, T., NAKAMOTO, T., KUTSUMIZU, S., YANO, S., and SORAI, M., 2002, *Phys. Rev. E*, **65,** 031719.
[31] KUTSUMIZU, S., ICHIKAWA, T., NOJIMA, S., and YANO, S., in Abstracts of ILCC 2000, Sendai, Japan, p. 114.
[32] LONGLEY, W., and MCINTOSH, T. J., 1983, *Nature*, **303,** 612.
[33] LARSSON, K., 1983, *Nature*, **304,** 664.
[34] GRAY, G. W., HARTLEY, J. B., and JONES, B., 1955, *J. chem. Soc.*, 1412.
[35] LUZZATI, V., and SPEGT, P. A., 1967, *Nature*, **215,** 701.
[36] KUTSUMIZU, S., YAMADA, M., TADANO, K., YANO, S., NOJIMA, S., and YAMAGUCHI, T., *Mol. Cryst. Liq. Cryst.* (submitted).
[37] RANÇON, Y., and CHARVOLIN, J., 1988, *J. phys. Chem.*, **92,** 2646.
[38] NISHINO, Y., YANO, S., TANSHO, M., and YAMAGUCHI, T., 1998, *Chem. Phys. Lett.*, **296,** 408.
[39] GÖRING, P., DIELE, S., FISHER, S., WIEGELEBEN, A., PELZL, G., STEGEMEYER, H., and THYEN, W., 1988, *Liq. Cryst.*, **25,** 467.
[40] SCHOEN, A. H., 1970, *NASA Tech. Note*, No. D-5541.
[41] ANDERSSON, S., HYDE, S. T., LARSSON, K., and LIDIN, S., 1988, *Chem. Rev.*, **88,** 221.
[42] HYDE, S. T., ANDERSSON, S., ERICSSON, B., and LARSSON, K., 1984, *Z. Kristallogr.*, **168,** 213.
[43] CLERC, M., and DUBOIS-VIOLETTE, E., 1994, *J. Phys. II Fr.*, **4,** 275.
[44] ISRAELACHVILI, J. N., 1985, *Intermolecular and Surface Forces* (London: Academic Press).
[45] SCHWARZ, U. S., and GOMPPER, G., 1999, *Phys. Rev. E*, **59,** 5528.